AGU PUBLICATIONS

Geophysical Research Letters

RESEARCH LETTER
10.1002/2015GL066753

Key Points:
- Anthropogenic aerosol deposition alleviates the nutrient limitation in the oceans
- Response of observed chlorophyll to anthropogenic aerosol deposition is modeled
- Over 1948–2007, the sensitivity of oceanic productivity to warming is reduced by 12.5%

Supporting Information:
- Supporting Information S1

Correspondence to:
R. Wang,
rong.wang@lsce.ipsl.fr

Citation:
Wang, R., et al. (2015), Influence of anthropogenic aerosol deposition on the relationship between oceanic productivity and warming, *Geophys. Res. Lett.*, *42*, 10,745–10,754, doi:10.1002/2015GL066753.

Received 26 OCT 2015
Accepted 18 NOV 2015
Accepted article online 24 NOV 2015
Published online 19 DEC 2015

Influence of anthropogenic aerosol deposition on the relationship between oceanic productivity and warming

Rong Wang[1,2,3], Yves Balkanski[1,3], Laurent Bopp[1,3], Olivier Aumont[4], Olivier Boucher[5], Philippe Ciais[1,3], Marion Gehlen[1,3], Josep Peñuelas[6,7], Christian Ethé[8], Didier Hauglustaine[1,3], Bengang Li[2,3], Junfeng Liu[2,3], Feng Zhou[2,3], and Shu Tao[2,3]

[1]Laboratoire des Sciences du Climat et de l'Environnement, CEA CNRS UVSQ, Gif-sur-Yvette, France, [2]Laboratory for Earth Surface Processes, College of Urban and Environmental Sciences, Peking University, Beijing, China, [3]Sino-French Institute for Earth System Science, College of Urban and Environmental Sciences, Peking University, Beijing, China, [4]Sorbonne Universités (UPMC, Université Paris 06)-CNRS-IRD-MNHN, LOCEAN-IPSL, Paris, France, [5]Laboratoire de Météorologie Dynamique, IPSL/CNRS, Université Pierre et Marie Curie, Paris, France, [6]CSIC, Global Ecology Unit CREAF-CEAB-UAB, Cerdanyola del Vallès, Catalonia, Spain, [7]CREAF, Cerdanyola del Vallès, Catalonia, Spain, [8]Laboratoire d'Oceanographie et de Climatologie, IPSL, Paris, France

Abstract Satellite data and models suggest that oceanic productivity is reduced in response to less nutrient supply under warming. In contrast, anthropogenic aerosols provide nutrients and exert a fertilizing effect, but its contribution to evolution of oceanic productivity is unknown. We simulate the response of oceanic biogeochemistry to anthropogenic aerosols deposition under varying climate from 1850 to 2010. We find a positive response of observed chlorophyll to deposition of anthropogenic aerosols. Our results suggest that anthropogenic aerosols reduce the sensitivity of oceanic productivity to warming from -15.2 ± 1.8 to -13.3 ± 1.6 Pg C yr^{-1} °C^{-1} in global stratified oceans during 1948–2007. The reducing percentage over the North Atlantic, North Pacific, and Indian Oceans reaches 40, 24, and 25%, respectively. We hypothesize that inevitable reduction of aerosol emissions in response to higher air quality standards in the future might accelerate the decline of oceanic productivity per unit warming.

1. Introduction

Marine net primary production (NPP) is a critical component of the Earth's carbon cycle, transferring some 50 Pg of carbon to the biosphere each year and important for sustaining the habitability of Earth [*Field et al.*, 1998; *Hoegh-Guldberg and Bruno*, 2010; *Boyce et al.*, 2010; *McNutt*, 2015; *Hoegh-Guldberg et al.*, 2014]. Field studies and model indicate a decline in oceanic NPP during 1998–2010 [*Behrenfeld et al.*, 2006; *Martinez et al.*, 2009; *Gregg and Rousseaux*, 2014], and this trend likely lasts throughout the twentieth century [*Boyce et al.*, 2010]. The decline is attributed mainly to the increasing thermal stratification of ocean water columns, induced by anthropogenic global warming. This increase in stability reduces the supply of nutrients from subsurface waters, thereby inhibiting the growth of phytoplankton [*Behrenfeld et al.*, 2006; *Martinez et al.*, 2009; *Boyce et al.*, 2010; *Gregg and Rousseaux*, 2014]. The process is simulated by ocean biogeochemical model [*Bopp et al.*, 2013] and is expected to continue further, reducing oceanic NPP. In contrast, anthropogenic aerosols provide nutrients to the surface oceans, which fertilize the phytoplankton and promote the oceanic NPP [*Jickells et al.*, 2005]. For example, by assuming complete assimilation of N in carbon fixation, *Duce et al.* [2008] estimated that contemporary deposition of anthropogenic nitrogen (N) can support a biological mediated carbon flux of ~0.3 Pg C yr^{-1} or ~3% relative to all new production in the oceans. A recent modeling study suggests that adding anthropogenic N and iron (Fe) deposition together can increase oceanic NPP by 1.5 Pg C yr^{-1} and reduces atmospheric CO_2 level by ~2.2 ppm by the year 2100 [*Krishnamurthy et al.*, 2009]. However, the impact of anthropogenic aerosol deposition (AAD) has not been simulated with the impact of climate change on stratification together in these models. *Mahowald et al.* [2011] used a coupled carbon climate model to study the effects of direct aerosol radiative forcing and Fe input from desert dust on the change of oceanic NPP under climate-induced changes in ocean. One of their main findings is that oceanic NPP increases following the input of Fe from desert dust and decreases as a consequence of the radiative effect of aerosols. In the present study, we quantify the fertilizing effect of anthropogenic aerosol deposition (i.e., not only Fe from dust) on the trend of

oceanic NPP under realistic climate over the last decades. Our purpose is to test the hypothesis that anthropogenic aerosol deposition can provide substantial nutrients and partly offset the decline of NPP caused by warming. To understand the impact of AAD, we simulated the change of N, Fe, and phosphorus (P) deposition from 1850 to 2010 in a global atmospheric general circulation model and input the results into an ocean biogeochemical model with the varying climate.

2. Data and Methods

2.1. Observational Data Sets

In this study, we compiled 182,552 in situ measurement data for the concentration of chlorophyll ([Chl]); 170,588 for nitrate (NO_3); 438,240 for phosphate (PO_4); and 214 data for soluble Fe (sFe), in the surface layer over open oceans (Figure S1 in the supporting information). In addition, the oceanic NPP for a period 1997–2007 from satellite were used to evaluate the spatial pattern of modeled NPP. More details are presented in Text S1.

2.2. Sources, Transport, and Deposition of N, P, and Fe in the Atmosphere

The global chemistry-aerosol-climate model LMDZ-OR-INCA couples online the LMDz (Laboratoire de Météorologie Dynamique, version 4) general circulation model [*Hourdin et al.*, 2006] and the INCA (INteraction with Chemistry and Aerosols, version 4) an aerosol module [*Hauglustaine et al.*, 2014]. This combination was run to simulate the global atmospheric emissions, transport, and deposition of N, P, and Fe. The models have been described in our previous papers [*Hauglustaine et al.*, 2014; *Wang et al.*, 2015a, 2015b] and detailed in Text S1.

The emissions of N, P, and Fe were compiled from 1850 to 2010. Global $0.5° \times 0.5°$ gridded monthly emissions of ammonia (NH_3) and nitrogen oxides (NO_x) from combustion and agriculture from 1850 to 2010 were taken from the ACCMIP and MACCity inventory [*Lamarque et al.*, 2010; *Granier et al.*, 2011]; the emissions of nitrogen oxide (NO) from soil and NH_3 from natural soils and oceans were estimated for present day in our model [*Hauglustaine et al.*, 2014] and assumed to be constant. The emissions of P and Fe from energy-related combustion and wildfires were estimated from 1960 to 2007 [*Wang et al.*, 2015a, 2015b]. These emissions were extrapolated by country from 1960 to 1850–1959 based on the sulfur emissions (less relying on technology change) in ACCMIP [*Lamarque et al.*, 2010] and from 2007 to 2008–2010 based on the black carbon emissions (sharing similar sources as P or Fe) in MACCity [*Granier et al.*, 2011]. The emissions of P and Fe from energy-related combustion were assumed to be constant throughout each year without seasonal variations. The monthly emissions from wildfires were calculated for 1960, 1970, 1980, 1990, and 2000 using the seasonal profile of black carbon emission from wildfires in each year [*Lamarque et al.*, 2010], for 2010 using the seasonal profile of black carbon emission from wildfires averaged over 2001–2008 [*Granier et al.*, 2011] and for 1850 using the seasonal profile of black carbon emission from wildfires averaged for 1960–1969 [*Lamarque et al.*, 2010]. Then, the monthly emissions of P and Fe in each country were disaggregated to $0.5° \times 0.5°$ grids using the $0.5° \times 0.5°$ distribution of corresponding black carbon emission [*Lamarque et al.*, 2010; *Granier et al.*, 2011]. The monthly emissions of Fe from dust (averaged over 2000–2011) and of P from dust (averaged over 2000–2011), primary biogenic aerosol particles (2000), and volcanoes (1990) were assumed to be constant throughout our study period, to isolate the impact of anthropogenic emissions.

We specified that 10% of P from dust, 100% of P from volcanoes, and 50% of P from other sources are converted to phosphate (PO_4), which is bioavailable [*Mahowald et al.*, 2008]. In addition, we applied the measured Fe solubility of $12 \pm 9\%$ for coal fly ash [*Fu et al.*, 2012; *Chen et al.*, 2012], $63.0 \pm 17.0\%$ for vehicle oil fly ash [*Oakes et al.*, 2012], $79.8 \pm 8.5\%$ for heavy oil fly ash [*Fu et al.*, 2012; *Schroth et al.*, 2009], $30 \pm 14\%$ for biomass ash [*Fu et al.*, 2012; *Oakes et al.*, 2012; *Bowie et al.*, 2009], and $2 \pm 4\%$ for dust [*Moore et al.*, 2004] to convert Fe to sFe, which is bioavailable. Snapshot simulations were performed to produce the monthly deposition of NO_3 and NH_4, PO_4, and sFe in 1850 and for snapshot years every tenth year from 1960 to 2010. All simulations were performed under present-day climate conditions nudging with the meteorological data for 2005 [*European Centre for Medium-Range Weather Forecasts (ECMWF)*, 2003]. The atmospheric deposition rates of NO_3 and NH_4, total Fe, and total P have been validated by in situ measurements [*Hauglustaine et al.*, 2014; *Wang et al.*, 2015a, 2015b]. The modeled surface-air concentrations of Fe and sFe have been validated by in situ measurements over the Atlantic and Pacific Oceans [*Wang et al.*, 2015b].

We performed a linear interpolation to obtain the deposition by month for each year between the two snapshot years.

2.3. A Global Ocean Biogeochemical Model

The monthly deposition of NO_3 and NH_4, PO_4, and sFe was prescribed in a state-of-the-art oceanic biogeochemical model NEMO-PISCES (version 2) [*Aumont et al.*, 2015], used to simulate the fate of nutrients (N, P, Fe, and silicon) and the carbon cycle in global oceans. The model can well capture the observed response of oceanic NPP to both dust [*Guieu et al.*, 2014] and climatic variability [*Schneider et al.*, 2008]. The model version and external sources of nutrients are detailed in Text S1. Major sources of DIN, PO_4, and sFe in the ocean are shown in Table S1.

2.4. Simulation Setup

In our study, the NEMO-PISCES model was run from 1768 to 2007, with the first 180 years as a spin-up. Simulations were forced by prescribed atmospheric levels of CO_2 from 1768 to 2007 [*Bopp et al.*, 2013]. Following Coordinated Ocean-ice Reference Experiments Phase II protocol [*Griffies et al.*, 2012], the recorded ocean forcing data from 1948 to 2007 [*Large and Yeager*, 2009] were used as input for the oceanic physical model, and the data were repeated in each 60 year period (Supporting Text). The monthly atmospheric deposition of NO_3 and NH_4, PO_4, and sFe was prescribed to the model. The simulation results were analyzed for the last 60 years from 1948 to 2007 with recorded forcing data.

We ran two simulations to study the impact of AAD: a control simulation (CTL) with the deposition fixed at the 1850 levels and an experimental simulation (DEP) with the deposition varying from 1850 to 2007. The difference was considered as the response to AAD.

3. Results

3.1. Sources and Oceanic Deposition of N, P, and Fe in Aerosols

Global emissions of reactive N (N_r, including NH_3 and NO_x), PO_4, and sFe for 1850–2010 are shown in Figures1a–1c. Total emissions of N_r, PO_4, and sFe have increased since 1850 by 181, 85, and 41%, respectively. Emissions of N_r, mainly from fossil fuels and agriculture, increased until 1990 and then leveled off due to the use of emission control devices for vehicles and industry. The energy-related emissions of PO_4 increased due to increasing contribution of biofuels to energy supply in developing countries and to deforestation in South America and Southeast Asia. Emissions of sFe from combustion rose before 1990 due to increased coal use and declined thereafter due to the implementation of industrial dust abatement facilities and the burning of cleaner fuels in the 1990s.

Emissions of N_r, PO_4, and sFe were prescribed in LMDZ-OR-INCA to obtain the oceanic deposition of dissolved inorganic N (DIN, including NO_3 and NH_4), PO_4, and sFe in 1850 and for annual snapshots every 10 years from 1960 to 2010 (Figures 1d–1f). Oceanic deposition of DIN, PO_4, and sFe has increased since 1850 by 137, 40, and 46%, respectively, mostly in the Northern Hemisphere. Deposition of DIN, PO_4, and sFe has increased by 310 (260%), 0.52 (110%), and 0.28 (200%) pmol m^{-2} s^{-1}, respectively, over the North Pacific and by 300 (230%), 0.11 (18%), and 0.030 (6%) pmol m^{-2} s^{-1}, respectively, over the North Atlantic (Figure S2). Our calculated DIN and sFe deposition is comparable to previous studies [*Duce et al.*, 2008; *Krishnamurthy et al.*, 2010], but our PO_4 deposition is higher due to larger P emissions for combustion sources [*Wang et al.*, 2015a].

3.2. Impact of AAD on Nutrients, Chlorophyll, and Productivity

NEMO-PISCES includes two types of phytoplankton, namely, nanophytoplankton and diatoms. The model simulates [Chl] and the growth of phytoplankton based on the availability of nutrients: PO_4, DIN, and sFe for nanophytoplankton and PO_4, DIN, sFe, and silicate for diatoms [*Aumont et al.*, 2015]. Hereafter, all results were derived by considering nanophytoplankton and diatoms together unless specified. Generally, the model accurately reproduces the spatial pattern of nutrient limitation of oceanic NPP for nanophytoplankton (Figures 2a and 2b). Over 1948–2007, the primary limiting nutrient for nanophytoplankton changes with an expansion of ocean areas limited by N, which took up 54% of total oceans in 1948–1977 and 57% in 1978–2007. In NEMO-PISCES, N is consumed by denitrification under suboxic conditions. It is likely that the projected declining oxygen content under warming [*Bopp et al.*, 2013] enhanced denitrification and caused a more stringent N limitation in the oceans (Figure S3). The model, however, does not properly resolve the observed colimitation by N and P over the North Atlantic and the Mediterranean Sea [*Moore et al.*, 2013]. Globally, 42% of the ocean is N limited,

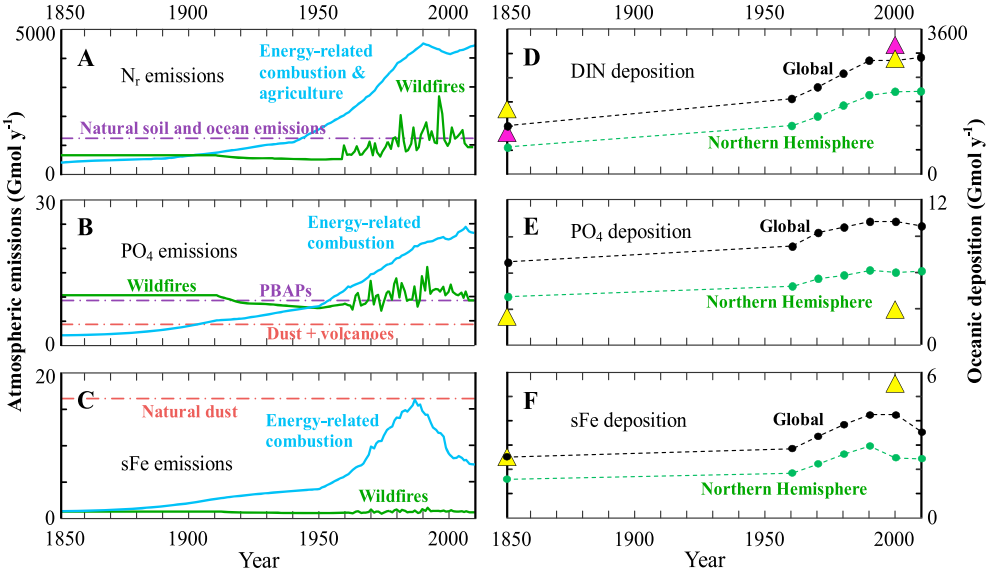

Figure 1. Atmospheric emissions and oceanic deposition of N, P, and Fe from 1850 to 2010. Emissions of (a) N_r, (b) PO_4, and (c) sFe from different sources ("PBAPs" stands for primary biogenic aerosol particles). Oceanic deposition of (d) DIN, (e) PO_4, and (f) sFe, for snapshot years (dots). Previous estimates of deposition are shown as purple [*Duce et al.*, 2008] or yellow [*Krishnamurthy et al.*, 2010] triangles.

similar to the 40% area found previously [*Krishnamurthy et al.*, 2007]; most of the remaining ocean is Fe limited. The pattern of nutrient limitation changes slightly from CTL to DEP corresponding to an alteration from N to P limitation in coastal oceans with high N depositions. In addition, we find an expansion of high-limitation region from DEP to CTL (contour lines in Figures 2a and 2b).

In the model, AAD increases the concentrations of DIN and sFe in the surface water (Figures 2c and 2d), alleviates nutrient limitation (contour lines in Figures 2a and 2b), increases [Chl] (Figure 2f), and enhances NPP (Figure 2g). The enhancement of phytoplankton growth in response to AAD corresponds to a supplementary PO_4 demand of 226 Gmol yr^{-1} averaged over 1948–2007. Since AAD provides only 9.3 Gmol yr^{-1} PO_4, meeting this demand yields an overall depletion of surface PO_4 as observed in Figure 2e. The largest relative impact of AAD on [Chl] and NPP is observed over the low-latitude Pacific. The absolute impact, however, differs from the relative impact, due to different background concentrations in different oceans (Figure S4). The frequency distribution of the relative difference between CTL and DEP simulations is computed for the surface concentrations of DIN, PO_4, sFe, [Chl], and NPP (Figure 2h). For example, the ocean area with a relative difference larger than 10% (a threshold selected for this analysis) takes up 65%, 50%, 50%, 34%, and 34% of all oceans for DIN, PO_4, sFe, [Chl], and NPP, respectively. Globally, as a fertilizing effect of anthropogenic N, P, and Fe deposition, the oceanic NPP was increased by 2.5% from 51.4 Pg C yr^{-1} in CTL to 52.7 Pg C yr^{-1} in DEP in 2007. Both estimates are within the uncertainty of the ocean color-based estimate of 40–60 Pg C yr^{-1} [*Carr et al.*, 2006]. If we consider solely nanophytoplankton, the NPP from nanophytoplankton was increased by 2.6%, respectively, for diatoms only, their NPP is increased by 2.0%, likely because diatoms require silicate for their growth.

Krishnamurthy et al. [2009] estimated that anthropogenic N and Fe deposition can increase oceanic NPP by 1.5 Pg C yr^{-1}. In comparison, by performing a sensitivity simulation with anthropogenic P only, we found that the oceanic NPP in 2007 decreased by 1.3 Pg C yr^{-1} relative to the DEP simulation, close to the estimate by *Krishnamurthy et al.* [2009]. However, some differences between our study and previously published results should be noted. For instance, our model predicts a different nutrient limitation spatial pattern over the subtropical North Atlantic in comparison with the one from *Krishnamurthy et al.* [2010] which suggests a large area limited by P under modern conditions. *Moore et al.* [2013] noticed that P can be seriously depleted over oligotrophic oceans in this region, but they noticed that adding P alone does not enhance NPP in deck incubations. *Okin et al.* [2011] assumed that P and Fe limitations can limit carbon fixation indirectly by limiting N fixation, but this effect is very sensitive to the N:Fe ratio in diazotrophic organisms. Therefore, the nutrient

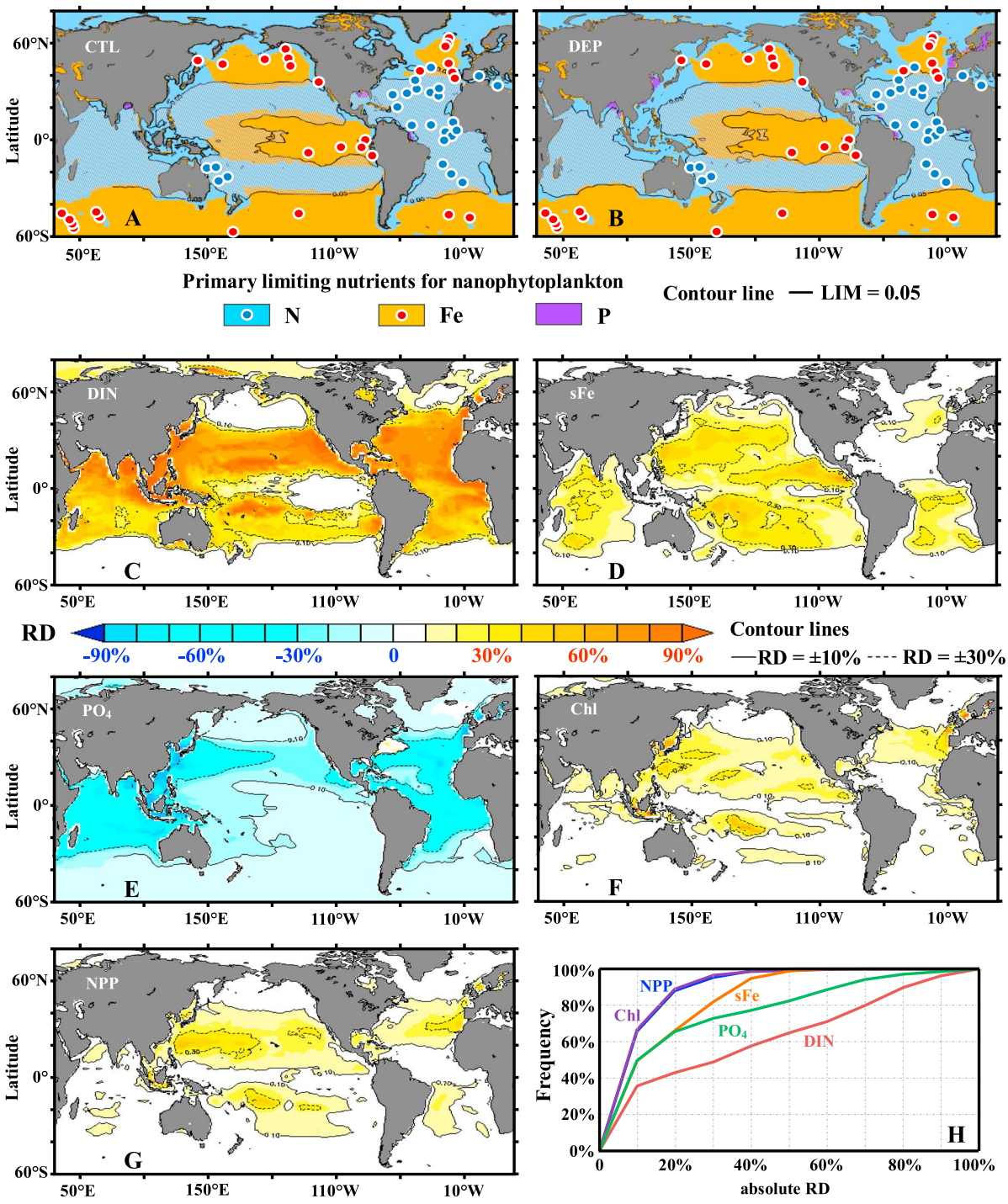

Figure 2. Impact of AAD on nutrients, [Chl], and NPP. Primary limiting nutrient for nanophytoplankton. In-fill color shows the element most frequently limiting nanophytoplanktonic growth by month during 1948–2007 (a) with or (b) without AAD. The contour line is for the modeled nutrient limitation factor (LIM) of 0.05. The shaded area indicates LIM < 0.05 with a stringent nutrient limitation. Observed limiting nutrients (circles) are from nutrient addition experiments [*Moore et al.*, 2013]. Influence of AAD on the modeled (c) DIN, (d) sFe, (e) PO_4, and (f) [Chl] and (g) NPP as DEP-CTL differences (RDs) relative to CTL for 1948–2007. RD is computed for the 0–30 m layer for nutrients and [Chl] and the 0–100 m layer for NPP. Contour lines are shown for RDs of ±10% (solid) and ±30% (dashed). (H) Frequency distribution of RD (negative for PO_4) in Figures 2c–2g. Comparison of modeled and observed [Chl] (i) with or (j) without (w/o) AAD. Plots are made in a log scale, with colors indicating the density of data in the panel. Number of sites (*n*), normalized mean bias (*NMB*), and root-mean-square deviation (*RMSD*) are shown. All measurement sites are divided into four quartiles of modeled [Chl] without AAD. [Chl] in the (k-m) first and (n–p) second quartiles are plotted against anthropogenic deposition (Dep.) of sFe (Figures 2k and 2n) or DIN (Figures 2l and 2o) and compared with the observations. [Chl] are averaged at an interval of 0.5 of ($\log_{10}$) deposition. The shaded areas show the difference modeled with or without AAD. The modeled [Chl] with anthropogenic deposition of only N (DEP-N), Fe (DEP-Fe), or P (DEP-P) are shown. Error bars show standard deviations of observed [Chl].

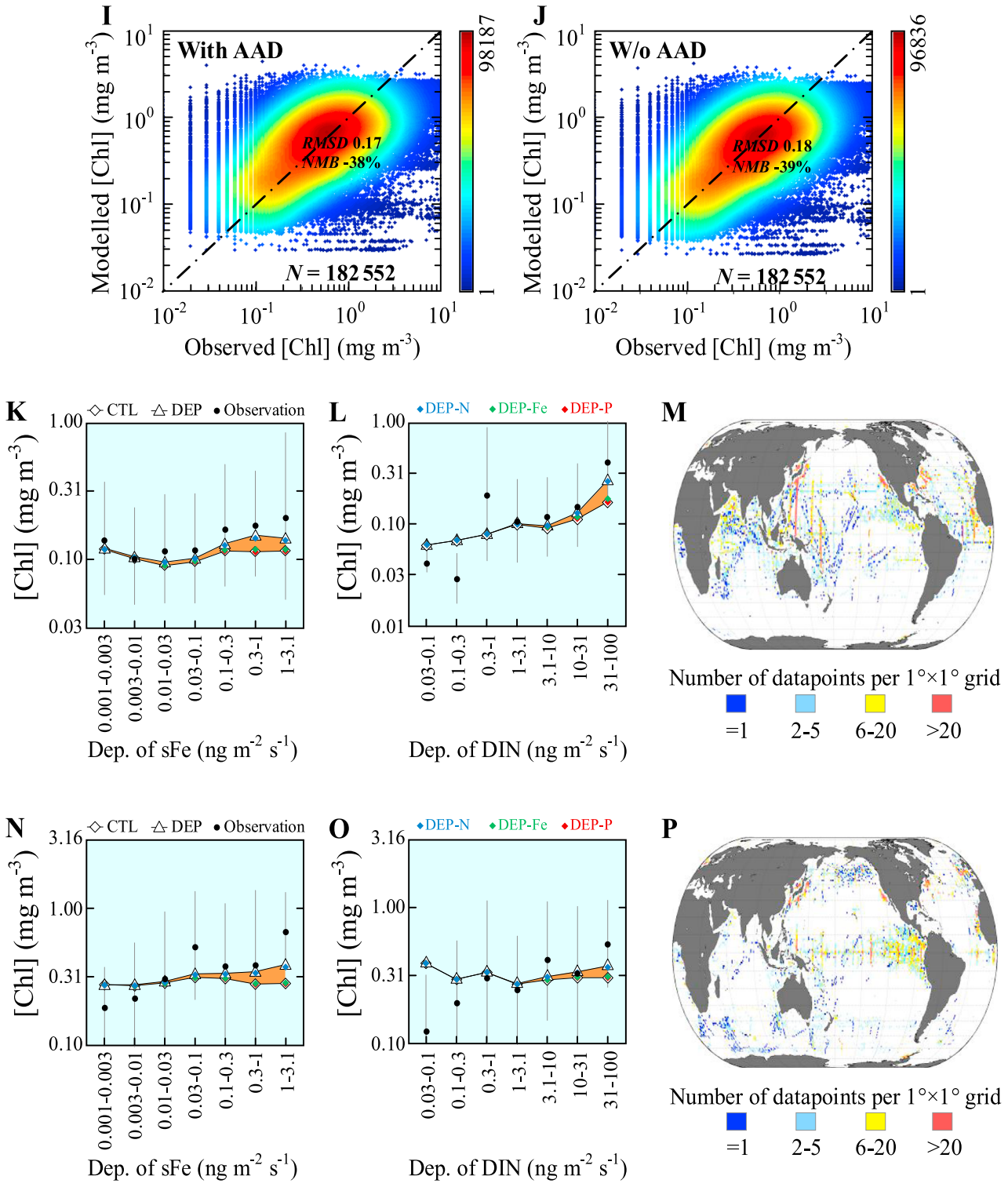

Figure 2. (continued)

colimitation should be better examined and studied in the future ocean models, and the effect of Fe could be underestimated if a high N:Fe ratio assumed by *Okin et al.* [2011] is confirmed.

3.3. Model-Data Comparison

The spatial pattern of modeled NPP is comparable to satellite-based estimates for 1997–2007 (Figure S5). The period covered by satellite observations is relatively short and corresponds to an era of intense anthropogenic aerosol emissions, making it difficult to detect the effect of AAD. In addition, the NPP difference modeled with or without AAD (Figure S5d) is very small relative to the total, making it difficult to identify a better or worse agreement between model and remote sensing data. Instead, we evaluated our model using in situ [Chl] measurements from 1948 to 2007. [Chl] does not have a simple relationship with NPP, but [Chl] and the rate of carbon fixation by phytoplankton both covary in response to environmental drivers. [Chl] is a valid indicator of oceanic NPP. We assembled a total of 182,552 measurements of [Chl] over the global oceans. Modeled [Chl] match the majority of observations, being around the 1:1 line (Figures 2i and 2j). However, adding AAD marginally improves the model-data comparison, with the normalized mean bias (NMB) and root-mean-square deviation (RMSD) changed from −39% and 0.18 to −38% and 0.17. In addition, by looking at sites where the relative difference of [Chl] between DEP and CTL is >10%, the NMB and RMSD were reduced from −42% and 0.24 to −32% and 0.17 ($n = 19\,0111$), respectively, possibly indicating an improvement at these sites (Figure S6). [Chl] in the oceans are evidently influenced by factors other than AAD, including ocean physics and other external factors such as interaction with sediments, river inputs, hydrothermalism, and deposition of natural dust [*Guieu et al.*, 2014; *Aumont et al.*, 2015]. The spatiotemporal distribution of [Chl] responds to changes in all these factors.

To isolate the response of [Chl] to AAD, we grouped all measurement sites into four quartiles based on the [Chl] modeled without AAD. In the first and second quartiles, the sites are more oligotrophic and sensitive to nutrient addition by AAD than those in the third and fourth quartiles. We plotted the [Chl] in the first and second quartiles against anthropogenic deposition of DIN or sFe (Figures 2k–2l), where the impact of AAD is shown as a shaded area. The modeled [Chl] at high N or Fe deposition sites are relatively high and agree better with the observations, consistent with a positive effect of AAD on [Chl] levels. Furthermore, sensitivity simulations with anthropogenic deposition of only N or P or Fe (diamonds in Figures 2n–2p) show that the effect of N is dominant, followed by Fe, and very weak for P on the [Chl] at high N or Fe deposition sites. This is reasonable as N is mostly the primary limiting nutrient at the sites close to continents where N or Fe deposition are elevated (Figures 2a and 2b). The effect of Fe deposition over the Fe-limited oceans far away from continents is less pronounced in our model. Lastly, a plot of [Chl] against AAD in the third and fourth quartiles of sites is shown in Figure S7. The impact of AAD is weak in these groups, suggesting that factors other than AAD are dominating the levels of [Chl].

Modeled NO_3, PO_4, and sFe concentrations were also compared against in situ measurements. Measurements of NO_3 and PO_4 below the detection limits (0.1 mmol m^{-3} for NO_3 and 0.03 mmol m^{-3} for PO_4) were not kept [*Patey et al.*, 2008], and we compared the modeled and observed NO_3 and PO_4 concentrations above a threshold. The RMSD and NMB for ($\log_{10}$) NO_3 concentrations decreased from 0.61 and −56% without AAD to 0.56 and −46% with AAD, respectively (Figure S8). The RMSD for ($\log_{10}$) PO_4 concentrations increased slightly from 0.45 to 0.46 with AAD. Detecting the impact of AAD on PO_4 requires further discrimination of reactive and nonreactive P in the model and data [*Karl et al.*, 1997]. In addition to the measurement bias, the underestimation of NO_3 and PO_4 in our standard simulation might be resulting from the Monod assumption for N and P, which deserves further studies by using the cell quota-based model [*Droop*, 1983]. The RMSD and NMB for ($\log_{10}$) sFe concentrations decreased from 0.63 and −68% to 0.57 and −63%, respectively (Figure S9). A more detailed discussion on the comparison of the nutrient distributions is presented in Text S1.

3.4. Long-Term Impact of AAD on Oceanic Productivity

Behrenfeld et al. [2006] found an inverse relationship of increasing sea surface temperature (SST) with decreasing NPP in the permanently stratified oceans from 1999 to 2004. We observed a similar relationship when comparing the period from 1948–1977 to 1978–2007(Figure S10). Furthermore, the correlations are equally as high with or without AAD (Figure 3), but including AAD decreases the sensitivity of NPP changes to SST changes. The slope of modeled NPP to observed SST decreased from -15.2 ± 1.8 (without AAD) to -13.3 ± 1.6 (with AAD) Pg C yr^{-1} °C^{-1}, a reduction by 12.5% relative to that without AAD. The North Pacific

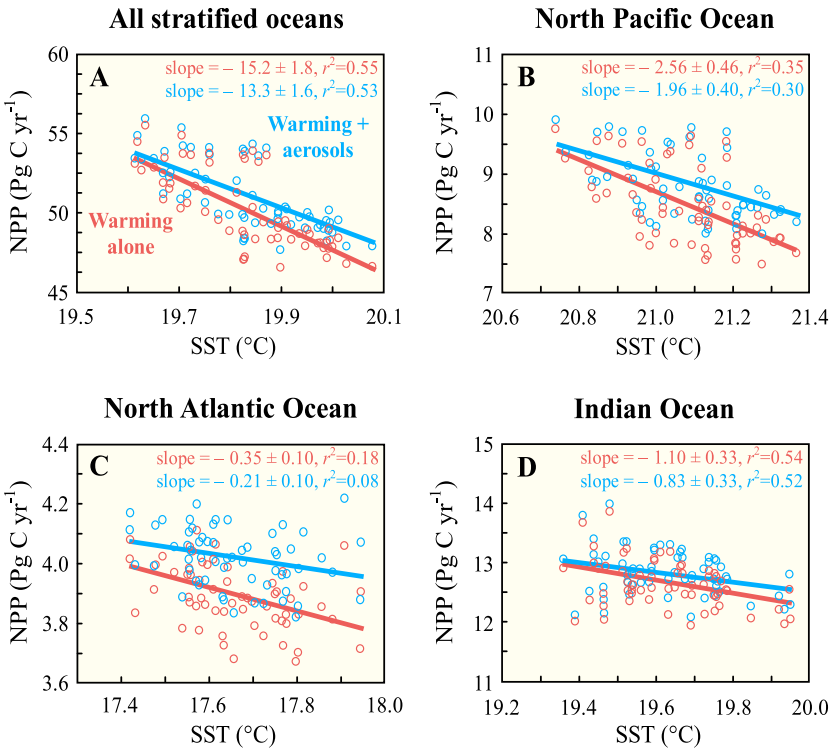

Figure 3. Relationship between annual NPP and SST for 1948–2007. NPP is computed in the model and SST is from the observations. (a) The permanently stratified oceans defined by *Behrenfeld et al.* [2006] are divided into (b) North Pacific, (c) North Atlantic, and (d) Indian Oceans. The circles show the relationship between NPP and SST under warming alone (red) or warming and AAD together (blue). The slope of NPP to SST (Pg C yr^{-1} °C^{-1}) and coefficient of determination (r^2) are estimated from least squares regression analysis.

has the largest change from -2.56 ± 0.46 to -1.96 ± 0.40 Pg C yr^{-1} °C^{-1}. The sensitivity of NPP to SST in the North Atlantic was reduced by 40% (-0.35 ± 0.10 to -0.21 ± 0.10 Pg C yr^{-1} °C^{-1}) by including AAD; this reduction was the largest, followed by the Indian Ocean (25%) and the North Pacific Ocean (24%). This percentage quantifies the offset of NPP sensitivity to SST by AAD. It depends on the response of NPP to AAD, as well as the sensitivity of NPP to SST. The largest percentage of change over North Atlantic is mainly due to the lowest NPP sensitivity to SST in the region.

Our finding has two major implications for future studies. First, any observation-based techniques to detect the influence of global warming on oceanic NPP have to take into account the role of AAD, as human-emitted aerosols can partly offset the effect of anthropogenic warming. Second, the evolution of aerosols deposition has to be considered when using the model to predict oceanic NPP. *Guieu et al.* [2014] found that the response of marine biota to a pulse change of atmospheric dust or N deposition occurs rapidly, while the duration of the perturbation is short (from a few days to two weeks) in the low nutrient low-chlorophyll (LNLC) oceans. We infer that marine biota in the LNLC oceans adjust rapidly to the AAD variation, in particular for deposition of N with a short turnover time (<1 month).

3.5. Limitations

In order to obtain a long-term effect of aerosols on ocean biogeochemistry, our estimate is subject to several sources of uncertainty, which should be addressed in the future study. First, we prescribed constant Fe solubility for each source from measurements without accounting for variability of Fe solubility under diverse atmospheric and ocean conditions [*Meskhidze et al.*, 2003; *Baker and Croot*, 2010]. Second, we did not include the emission of dust from land cover change, and the impact should be considered when this global source is better understood [*Neff et al.*, 2008; *Ginoux et al.*, 2012]. Third, we did not derive the daily atmospheric input from 1850 to 2010 due to heavy computational load. As a result, the monthly resolution of nutrient

deposition cannot capture episodic transport [*Guieu et al.*, 2014]. Fourth, our model did not include the toxic effect of anthropogenic heavy metals. For example, *Paytan et al.* [2009] predicted a remarkable toxic effect of anthropogenic copper over the Bay of Bengal and downwind of South and East Asia close to the land with a limited impact over the remote oceans.

4. Conclusion and Implications

Marine ecosystems are sensitive to environmental changes [*Hoegh-Guldberg et al.*, 2014; *McNutt*, 2015]. Global warming induced by greenhouse gases emissions has increased ocean stratification and reduced nutrient supply for phytoplankton in the surface ocean [*Behrenfeld et al.*, 2006; *Boyce et al.*, 2010]. The most important findings of our study are that (1) the fertilizing effects of aerosols should be considered along with the effects of climate change and variability in driving NPP variations and (2) anthropogenic N deposition dominates the fertilizing effect of aerosols. Nonetheless, the effects of Fe and P deserve more studies, in particular they can alter the N cycle in the oceans and impact on NPP. Our study identifies anthropogenic aerosols deposition as an overlooked factor that can compensate partly the decline of nutrients induced by warming. A recent study reported that ambient aerosol pollution led to ~3 million premature deaths in 2010 [*Lim et al.*, 2013], so these emissions will inevitably be controlled [*Shindell et al.*, 2012], likely before 2030 in the major emitting countries in Asia [*S. X. Wang et al.*, 2014, *R. Wang et al.*, 2014]. According to the Representative Concentration Pathways scenarios [*Lamarque et al.*, 2011], the emissions of NO_x and sulfur (sharing similar sources as P and Fe) will decrease by 34–59% and 75–88% from 2010 to 2100, although ammonia will increase by 3–55%. If our analysis proves robust, higher air quality standards, while improving air quality, will reduce atmospheric deposition of nutrients and accelerate decline in oceanic NPP due to warming. Such changes will have impacts on marine food webs and the global carbon and nitrogen cycles and climate.

Acknowledgments

The authors thank Ether/ECCAD for the distribution of emission data used in this study. The authors acknowledge Alex Baker, Marco van Hulten, and Shilong Piao for their useful comments and John Gash for editing the English. R. W. was supported by the FABIO project, a Marie Curie International Incoming Fellowship from European Commission (PIIF-GA-2013-628735). This work was also conducted as part of the IMBALANCE-P project of the European Research Council (ERC-2013-SyG-610028). Some of the computations were performed using HPC resources from GENCI-TGCC (grant 2015-t2015012201). F.Z. was supported by the National Natural Science Foundation of China (grant 41201077). The version of the NEMO-PISCES code used in this study is freely available at http://www.nemo-ocean.eu/.

References

Aumont, O., C. Ethé, A. Tagliabue, L. Bopp, and M. Gehlen (2015), PISCES-v2: An ocean biogeochemical model for carbon and ecosystem studies, *Geosci. Model Dev.*, *8*, 2465–2513, doi:10.5194/gmd-8-2465-2015.

Baker, A. R., and P. L. Croot (2010), Atmospheric and marine controls on aerosol iron solubility in seawater, *Mar. Chem.*, *120*(1), 4–13, doi:10.1016/j.marchem.2008.09.003.

Behrenfeld, M. J., R. T. O'Malley, D. A. Siegel, C. R. McClain, J. L. Sarmiento, G. C. Feldman, A. J. Milligan, P. G. Falkowski, R. M. Letelier, and E. S. Boss (2006), Climate-driven trends in contemporary ocean productivity, *Nature*, *444*, 752–755, doi:10.1038/nature05317.

Bopp, L., et al. (2013), Multiple stressors of ocean ecosystems in the 21st century: Projections with CMIP5 models, *Biogeosciences*, *10*, 6225–6245, doi:10.5194/bg-10-6225-2013.

Bowie, A. R., D. Lannuzel, T. A. Remenyi, T. Wagener, P. J. Lam, P. W. Boyd, C. Guieu, A. T. Townsend, and T. W. Trull (2009), Biogeochemical iron budgets of the Southern Ocean south of Australia: Decoupling of iron and nutrient cycles in the subantarctic zone by the summertime supply, *Global Biogeochem. Cycles*, *23*, GB4034, doi:10.1029/2009GB003500.

Boyce, D. G., M. R. Lewis, and B. Worm (2010), Global phytoplankton decline over the past century, *Nature*, *466*, 591–596, doi:10.1038/nature09268.

Carr, M. E., et al. (2006), A comparison of global estimates of marine primary production from ocean color, *Deep Sea Res., Part II*, *53*, 741–770.

Chen, H., A. Laskin, J. Baltrusaitis, C. A. Gorski, M. M. Scherer, and V. H. Grassian (2012), Coal fly ash as a source of iron in atmospheric dust, *Environ. Sci. Technol.*, *46*, 2112–2120, doi:10.1021/es204102f.

Droop, M. R. (1983), 25 years of algal growth kinetics, *Bot. Mar.*, *26*, 99–112.

Duce, R. A., et al. (2008), Impacts of atmospheric anthropogenic nitrogen on the open ocean, *Science*, *320*, 893–897, doi:10.1126/science.1150369.

ECMWF (European Centre for Medium-Range Weather Forecasts) (2003), Forty-year European reanalysis of the global atmosphere. [Available at www.ecmwf.int/products/, Accessed November 6, 2013.]

Field, C. B., M. J. Behrenfeld, J. T. Randerson, and P. Falkowski (1998), Primary production of the biosphere: Integrating terrestrial and oceanic components, *Science*, *281*, 237–240, doi:10.1126/science.281.5374.237.

Fu, H., J. Lin, G. Shang, W. Dong, V. H. Grassian, G. R. Carmichael, Y. Li, and J. Chen (2012), Solubility of iron from combustion source particles in acidic media linked to iron speciation, *Environ. Sci. Technol.*, *46*, 11,119–11,127, doi:10.1021/es302558m.

Ginoux, P., J. M. Prospero, T. E. Gill, N. C. Hsu, and M. Zhao (2012), Global scale attribution of anthropogenic and natural dust sources and their emission rates based on MODIS Deep Blue aerosol products, *Rev. Geophys.*, *50*, RG3005, doi:10.1029/2012RG000388.

Granier, C., et al. (2011), Evolution of anthropogenic and biomass burning emissions of air pollutants at global and regional scales during the 1980–2010 period, *Clim. Change*, *109*, 163–190, doi:10.1007/s10584-011-0154-1.

Gregg, W. W., and C. S. Rousseaux (2014), Decadal trends in global pelagic ocean chlorophyll: A new assessment integrating multiple satellites, in situ data, and models, *J. Geophys. Res. Oceans*, *119*, 5921–5933, doi:10.1002/2014JC010158.

Griffies, S. M., S. M. Griffies, M. Winton, B. Samuels, G. Danabasoglu, S. Yeager, S. Marlsand, H. Drange, and M. Bentsen (2012), Datasets and protocol for the CLIVAR WGOMD Coordinated Ocean-sea ice Reference Experiments (COREs) (WCRP Report No. 21).

Guieu, C., et al. (2014), The significance of the episodic nature of atmospheric deposition to Low Nutrient Low Chlorophyll regions, *Global Biogeochem. Cycles*, *28*, 1179–1198, doi:10.1002/2014GB004852.

Hauglustaine, D. A., Y. Balkanski, and M. Schulz (2014), A global model simulation of present and future nitrate aerosols and their direct radiative forcing of climate, *Atmos. Chem. Phys.*, *14*, 11,031–11,063, doi:10.5194/acp-14-11031-2014.

Hoegh-Guldberg, O., and J. F. Bruno (2010), The impact of climate change on the world's marine ecosystems, *Science*, *328*, 1523–1528, doi:10.1126/science.1189930.

Hoegh-Guldberg, O., et al. (2014), *The Ocean*, Cambridge Univ. Press, Cambridge, U. K., and New York.

Hourdin, F., et al. (2006), The LMDZ4 general circulation model: Climate performance and sensitivity to parametrized physics with emphasis on tropical convection, *Clim. Dynam.*, *27*, 787–813, doi:10.1007/s00382-006-0158-0.
Jickells, T. D., et al. (2005), Global iron connections between desert dust, ocean biogeochemistry, and climate, *Science*, *308*, 67–71, doi:10.1126/science.1105959.
Karl, D., R. Letelier, L. Tupas, J. Dore, J. Christian, and D. Hebel (1997), The role of nitrogen fixation in biogeochemical cycling in the subtropical North Pacific Ocean, *Nature*, *388*, 533–538.
Krishnamurthy, A., J. K. Moore, C. S. Zender, and C. Luo (2007), Effects of atmospheric inorganic nitrogen deposition on ocean biogeochemistry, *J. Geophys. Res.*, *112*, G02019, doi:10.1029/2006JG000334.
Krishnamurthy, A., J. K. Moore, N. Mahowald, C. Luo, S. C. Doney, K. Lindsay, and C. S. Zender (2009), Impacts of increasing anthropogenic soluble iron and nitrogen deposition on ocean biogeochemistry, *Global Biogeochem. Cycles*, *23*, GB3016, doi:10.1029/2008GB003440.
Krishnamurthy, A., J. K. Moore, N. Mahowald, C. Luo, and C. S. Zender (2010), Impacts of atmospheric nutrient inputs on marine biogeochemistry, *J. Geophys. Res.*, *115*, G01006, doi:10.1029/2009JG001115.
Lamarque, J. F., et al. (2010), Historical (1850–2000) gridded anthropogenic and biomass burning emissions of reactive gases and aerosols: methodology and application, *Atmos. Chem. Phys.*, *10*, 7017–7039, doi:10.5194/acp-10-7017-2010.
Lamarque, J. F., G. P. Kyle, M. Meinshausen, K. Riahi, S. J. Smith, D. P. van Vuuren, A. J. Conley, and F. Vitt (2011), Global and regional evolution of short-lived radiatively-active gases and aerosols in the Representative Concentration Pathways, *Clim. Change*, *109*, 191–212, doi:10.1007/s10584-011-0155-0.
Large, W. G., and S. G. Yeager (2009), The global climatology of an interannually varying air-sea flux data set, *Clim. Dynam.*, *33*, 341–364, doi:10.1007/s00382-008-0441-3.
Lim, S. S., et al. (2013), A comparative risk assessment of burden of disease and injury attributable to 67 risk factors and risk factor clusters in 21 regions, 1990–2010: a systematic analysis for the Global Burden of Disease Study 2010, *Lancet*, *380*, 2224–2260, doi:10.1016/S0140-6736(12)61766-8.
Mahowald, N., et al. (2008), Global distribution of atmospheric phosphorus sources, concentrations and deposition rates, and anthropogenic impacts, *Global Biogeochem. Cycles*, *22*, GB4026, doi:10.1029/2008GB003240.
Mahowald, N., K. Lindsay, D. Rothenberg, S. C. Doney, J. K. Moore, P. Thornton, J. T. Randerson, and C. D. Jones (2011), Desert dust and anthropogenic aerosol interactions in the Community Climate System Model coupled-carbon-climate model, *Biogeosciences*, *8*, 387–414, doi:10.5194/bg-8-387-2011.
Martinez, E., D. Antoine, F. D'Ortenzio, and B. Gentili (2009), Climate-driven basin-scale decadal oscillations of oceanic phytoplankton, *Science*, *326*, 1253–1256, doi:10.1126/science.1177012.
McNutt, M. (2015), Oceans and Earth's habitability, *Science*, *348*, 841–841, doi:10.1126/science.aac5755.
Meskhidze, N., W. L. Chameides, A. Nenes, and G. Chen (2003), Iron mobilization in mineral dust: Can anthropogenic SO_2 emissions affect ocean productivity? *Geophys. Res. Lett.*, *30*(21), 2085, doi:10.1029/2003GL018035.
Moore, C. M., et al. (2013), Processes and patterns of oceanic nutrient limitation, *Nat. Geosci.*, *6*, 701–710, doi:10.1038/ngeo1765.
Moore, J. K., S. C. Doney, and K. Lindsay (2004), Upper ocean ecosystem dynamics and iron cycling in a global three-dimensional model, *Global Biogeochem. Cycles*, *18*, GB4025, doi:10.1029/2004GB002220.
Neff, J. C., A. P. Ballantyne, G. L. Farmer, N. M. Mahowald, J. L. Conroy, C. C. Landry, J. T. Overpeck, T. H. Painter, C. R. Lawrence, and R. L. Reynolds (2008), Increasing eolian dust deposition in the western United States linked to human activity, *Nat. Geosci.*, *1*, 189–195, doi:10.1038/ngeo133.
Oakes, M., E. D. Ingall, B. Lai, M. M. Shafer, M. D. Hays, Z. G. Liu, A. G. Russell, and R. J. Weber (2012), Iron solubility related to particle sulfur content in source emission and ambient fine particles, *Environ. Sci. Technol.*, *46*, 6637–6644, doi:10.1021/es300701c.
Okin, G. S., et al. (2011), Impacts of atmospheric nutrient deposition on marine productivity: Roles of nitrogen, phosphorus, and iron, *Global Biogeochem. Cycles*, *25*, GB2022, doi:10.1029/2010GB003858.
Patey, M. D., M. J. A. Rijkenberg, P. J. Statham, M. C. Stinchcombe, and E. P. Achterberg (2008), Determination of nitrate and phosphate in seawater at nanomolar concentrations, *TrAC, Trends Anal. Chem.*, *27*, 169–182, doi:10.1016/j.trac.2007.12.006.
Paytan, A., et al. (2009), Toxicity of atmospheric aerosols on marine phytoplankton, *Proc. Natl. Acad. Sci. U.S.A.*, *106*, 4601–4605, doi:10.1073/pnas.0811486106.
Schneider, B., et al. (2008), Climate-induced interannual variability of marine primary and export production in three global coupled climate carbon cycle models, *Biogeosciences*, *5*, 597–614, doi:10.5194/bg-5-597-2008.
Schroth, A. W., J. Crusius, E. R. Sholkovitz, and B. C. Bostick (2009), Iron solubility driven by speciation in dust sources to the ocean, *Nat. Geosci.*, *2*, 337–340, doi:10.1038/ngeo501.
Shindell, D., et al. (2012), Simultaneously mitigating near-term climate change and improving human health and food security, *Science*, *335*, 183–189, doi:10.1126/science.1210026.
Wang, R., et al. (2014), Exposure to ambient black carbon derived from a unique inventory and high resolution model, *Proc. Natl. Acad. Sci. U.S.A.*, *111*, 2459–2463, doi:10.1073/pnas.1318763111.
Wang, R., Y. Balkanski, O. Boucher, P. Ciais, J. Peñuelas, and S. Tao (2015a), Significant contribution of combustion-related emissions to the atmospheric phosphorus budget, *Nat. Geosci.*, *8*, 48–54, doi:10.1038/ngeo2324.
Wang, R., Y. Balkanski, O. Boucher, L. Bopp, A. Chappell, P. Ciais, D. Hauglustaine, J. Peñuelas, and S. Tao (2015b), Sources, transport and deposition of iron in the global atmosphere, *Atmos. Chem. Phys.*, *15*, 6247–6270, doi:10.5194/acp-15-6247-2015.
Wang, S. X., et al. (2014), Emission trends and mitigation options for air pollutants in East Asia, *Atmos. Chem. Phys.*, *14*, 6571–6603, doi:10.5194/acp-14-6571-2014.